

SDSS J1029+2623: A GRAVITATIONALLY LENSED QUASAR WITH AN IMAGE SEPARATION OF 22.5 ARCSECONDS¹

NAOHISA INADA^{2,3}, MASAMUNE OGURI^{4,5}, TOMOKI MOROKUMA², MAMORU DOI², NAOKI YASUDA⁶, ROBERT H. BECKER^{7,8}, GORDON T. RICHARDS^{9,10}, CHRISTOPHER S. KOCHANEK¹¹, ISSHA KAYO¹², KOHKI KONISHI⁶, HIROYUKI UTSUNOMIYA², MIN-SU SHIN⁵, MICHAEL A. STRAUSS⁵, ERIN S. SHELDON¹³, DONALD G. YORK^{14,15}, JOSEPH F. HENNAWI¹⁶, DONALD P. SCHNEIDER¹⁷, XINYU DAI¹¹, AND MASATAKA FUKUGITA⁶

Draft version September 10, 2018

ABSTRACT

We report the discovery of a cluster-scale lensed quasar, SDSS J1029+2623, selected from the Sloan Digital Sky Survey. The lens system exhibits two lensed images of a quasar at $z_s = 2.197$. The image separation of 22''.5 makes it the largest separation lensed quasar discovered to date. The similarity of the optical spectra and the radio loudnesses of the two components support the lensing hypothesis. Images of the field show a cluster of galaxies at $z_l \sim 0.55$ that is responsible for the large image separation. The lensed images and the cluster light center are not collinear, which implies that the lensing cluster has a complex structure.

Subject headings: gravitational lensing — quasars: individual (SDSS 102913.94+262317.9) — galaxies: clusters: general

1. INTRODUCTION

The discovery of SDSS J1004+4112 with an image separation of 14''.6, the first example of a quasar multiply imaged by a massive cluster of galaxies, opened a new window for understanding our universe (Inada et al. 2003; Oguri et al. 2004; Sharon et al. 2005). Although there are many examples of galaxies (arcs) lensed by clusters, large-separation lensed quasars have several advantages over arcs as a cosmological probe. First, the simpler (point-like) structure of quasars and their well-understood redshift distribution should make the large-

separation lensed quasars much cleaner probes of cosmology and structure formation models (e.g., Oguri & Keeton 2004; Hennawi et al. 2006), while the statistics of arcs remain contentious (Bartelmann et al. 2003). Second, the time-variability of quasars allows the measurement of time delays among the multiple lensed images, thereby breaking the mass-sheet degeneracy of lens models given a priori knowledge of the Hubble constant (e.g., Kochanek 2002). This was explored in detail for SDSS J1004+4112 (e.g., Oguri et al. 2004; Williams & Saha 2004; Kawano & Oguri 2006; Fohlmeister et al. 2006). Our current problem is that the small number of known systems limits their use in statistical analyses, however, current and future large lens surveys will discover many large-separation lensed quasars (Wambsganss 2003).

In this *Letter*, we report the discovery of the second large-separation lensed quasar, SDSS J1029+2623, a quasar at $z_s = 2.197$ doubly imaged by a massive galaxy cluster at $z_l \sim 0.55$. It was discovered in the course of the Sloan Digital Sky Survey Quasar Lens Search (SQLS; Oguri et al. 2006), which is a survey of strongly lensed quasars in the Sloan Digital Sky Survey (SDSS; York et al. 2000). The image separation of 22''.5 makes it the largest separation lens among the ~ 100 lensed quasars known so far (Kochanek 2006).

2. CANDIDATE SELECTION AND SUBARU OBSERVATIONS

From the SDSS-II Sloan Legacy Survey data, we discovered the lens candidate SDSS J1029+2623 using the algorithm described in Oguri et al. (2006). It consists of a quasar whose redshift was spectroscopically measured by the SDSS to be $z = 2.198$ (hereafter referred to as A) and a stellar object (hereafter B) with almost the same color as component A (see Table 1). Components A and B are separated by 22''.5. There are no other point sources in the field with similar colors that would be candidates for additional quasar images. In addition to the similar colors, the *gri* composite SDSS image shown in the left panel of Figure 1 exhibits a concentration of red galaxies centered on two bright galaxies (named G1 and

arXiv:astro-ph/0611275v1 8 Nov 2006

¹ Based in part on data collected at Subaru Telescope, which is operated by the National Astronomical Observatory of Japan.

² Institute of Astronomy, Faculty of Science, University of Tokyo, 2-21-1 Osawa, Mitaka, Tokyo 181-0015, Japan.

³ Japan Society for the Promotion of Science (JSPS) Research Fellow.

⁴ Kavli Institute for Particle Astrophysics and Cosmology, Stanford University, 2575 Sand Hill Road, Menlo Park, CA 94025.

⁵ Princeton University Observatory, Peyton Hall, Princeton, NJ 08544.

⁶ Institute for Cosmic Ray Research, University of Tokyo, 5-1-5 Kashiwa, Kashiwa, Chiba 277-8582, Japan.

⁷ IGPP-LLNL, L-413, 7000 East Avenue, Livermore, CA 94550.

⁸ Department of Physics, University of California at Davis, 1 Shields Avenue, Davis, CA 95616.

⁹ Department of Physics, Drexel University, 3141 Chestnut Street, Philadelphia, PA 19104.

¹⁰ Johns Hopkins University, 3400 N. Charles St., Baltimore, MD 21218.

¹¹ Department of Astronomy, The Ohio State University, Columbus, OH 43210.

¹² Department of Physics and Astrophysics, Nagoya University, Chikusa-ku, Nagoya 464-8062, Japan.

¹³ Center for Cosmology and Particle Physics, Department of Physics, New York University, 4 Washington Place, New York, NY 10003.

¹⁴ Department of Astronomy and Astrophysics, The University of Chicago, 5640 South Ellis Avenue, Chicago, IL 60637.

¹⁵ Enrico Fermi Institute, The University of Chicago, 5640 South Ellis Avenue, Chicago, IL 60637.

¹⁶ Department of Astronomy, University of California at Berkeley, 601 Campbell Hall, Berkeley, CA 94720-3411.

¹⁷ Department of Astronomy and Astrophysics, The Pennsylvania State University, 525 Davey Laboratory, University Park, PA 16802.

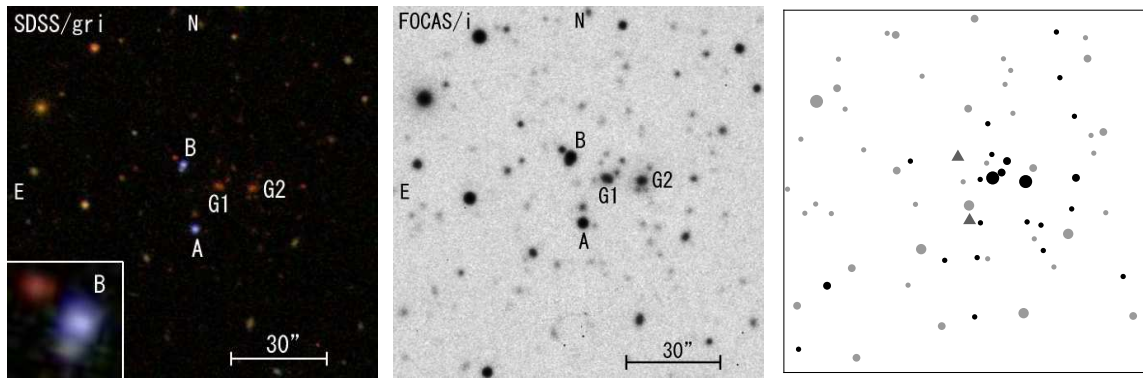


FIG. 1.— *Left*: The *gri* composite SDSS image of SDSS J1029+2623 ($1''.3$ seeing). The quasar images (blue stellar objects) are indicated by A and B. G1 and G2 (red extended objects) are likely to be member galaxies of a lensing cluster at $z \sim 0.55$. The inset shows an expanded view of component B: An object $\sim 2''$ Southeast of component B has quite different color from those of the quasar components. *Middle*: The FOCAS *i*-band image ($1''.8$ seeing). *Right*: Locations of galaxies ($i < 22.5$) identified in the FOCAS images are plotted with filled circles. Larger circles mean brighter galaxies. Galaxies that survive the color cut of $R - i = 0.7 \pm 0.3$ are shown by darker circles. Filled triangles are the locations of the two quasar images. In all the panels, North is up and East is left.

G2), which implies the existence of a high-redshift cluster of galaxies. Indeed, the photometric redshifts of G1 and G2 are both ~ 0.55 from their SDSS colors (Csabai et al. 2003). The properties of components A, B, G1, and G2 are summarized in Table 1. We note that the details of the SDSS are described in a series of technical papers: Gunn et al. (2006) for the dedicated wide-field (3° field of view) 2.5-m telescope; Fukugita et al. (1996), Gunn et al. (1998), Lupton et al. (1999), Hogg et al. (2001), Lupton et al. (2001), Smith et al. (2002), Pier et al. (2003), Ivezić et al. (2004), and Tucker et al. (2006) for the photometric survey; Richards et al. (2002) for the spectroscopic target selection algorithm of quasars; and Blanton et al. (2003) for the tiling algorithm of the spectroscopic survey. Most of the SDSS data are already publicly available (Stoughton et al. 2002; Abazajian et al. 2003, 2004, 2005; Adelman-McCarthy et al. 2006).

We obtained 600 sec spectra of components A and B with the Faint Object Camera And Spectrograph (FOCAS; Kashikawa et al. 2002) at the Subaru 8.2-meter telescope on 2006 June 28. The observation was conducted in the 3×1 on-chip binning mode, using the 300B grism, the SY47 filter and a $0''.8$ -width slit aligned along components A and B. The spectral resolution, wavelength coverage, and spatial scale of the CCD detector were $R \sim 500$, from 4700 \AA to 9400 \AA , and $0''.311 \text{ pixel}^{-1}$, respectively. Although the seeing was poor ($\sim 1''.8$), the $22''.5$ separation makes it easy to extract the spectra of the two components using standard IRAF¹⁸ tasks. The spectra are shown in the upper panel of Figure 2. It is clear that both components are quasars at the same redshift, $z = 2.197$ (see Table 1). Moreover, the spectral shapes are similar; both components have similar broad absorption line features at the same wavelength in the C IV emission lines, similar profiles for the Fe III emission lines, and similar characteristic shapes of the red wings of the Mg II emission lines. In addition, the spectral flux ratio plotted in the lower panel of Figure 2 is constant (~ 1.2) over the full range of the observed wavelengths. The similarity of the spectra supports the idea that the two components are lensed images of a single

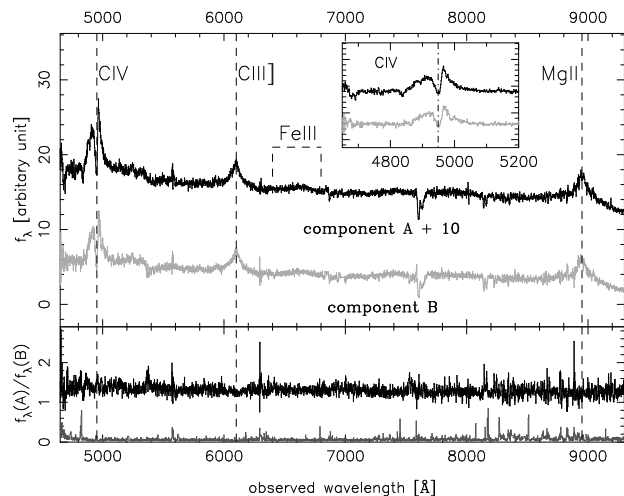


FIG. 2.— Spectra of components A (black solid line, shifted upwards by a constant of 10 flux density units) and B (gray solid line) taken with the FOCAS on the Subaru telescope. The signal to noise ratio (in the $6000 \text{ \AA} - 8000 \text{ \AA}$ continuum) is about 25.0 per pixel. The dotted lines indicate the positions of the quasar C IV, C III], Fe III, and Mg II emission lines redshifted to $z = 2.197$. The feature at 7600 \AA is atmospheric. The inset shows an expanded view of the C IV emission lines. The vertical dot-dashed line in the inset shows the central position of the broad absorption lines. In the bottom panel, the black solid line shows the spectral flux ratio between A and B, and the dark gray solid line shows the 1σ error of the spectral flux ratio, which is derived from the noise per pixel in each spectrum. The ratio is confirmed to be constant (~ 1.2) within the 2.3σ error, over the entire range of observed wavelengths.

quasar.

We also obtained 120 sec *R*- and 120 sec *i*-band images ($\sim 1''.8$ seeing) with FOCAS. On-chip 2×2 binning yielded images with a pixel scale of $0''.207 \text{ pixel}^{-1}$. The *i*-band image is shown in the middle panel of Figure 1. From the FOCAS images, we found that galaxy G1 is likely to be a superposition of two early-type galaxies; however, we treated them as a single object since the poor seeing prevents us from separating them. We used SExtractor (Bertin & Arnouts 1996) for the photometry (MAG_AUTO) calibrated by the SDSS magnitudes of the nearby stars¹⁹. All galaxies (classified by the com-

¹⁸ IRAF is distributed by the National Optical Astronomy Observatories, which are operated by the Association of Universities for Research in Astronomy, Inc., under cooperative agreement with the National Science Foundation.

¹⁹ We used the transformation formulae described in Table 7 of Smith et al. (2002) to calculate *R* magnitudes of the nearby stars from the SDSS *gr* magnitudes.

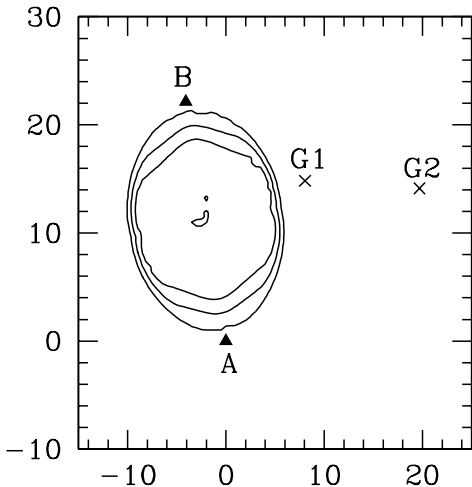


FIG. 3.— Constraints on the center of the potential of the lensing cluster from mass modeling. Solid lines indicate 1, 2, and 3σ likelihood regions for the center based on an SIE model for the cluster potential (see text for details). The quasar images (A and B) and bright member galaxies (G1 and G2) are marked by filled triangles and crosses, respectively. If we model the system using a SIE+external shear with the potential center fixed to galaxy G1, the best-fitting model has an Einstein radius of $15''.0$ (corresponding to the velocity dispersion of $\sim 900 \text{ km sec}^{-1}$), an ellipticity of 0.25 with its direction of 88° (East of North), and a shear of 0.09 with its direction of 28° , although it does not reproduce the observables exactly.

bination of the SExtractor CLASS_STAR parameter and visual inspection) with $i < 22.5$ are plotted as filled circles in the right panel of Figure 1. Among them, we selected galaxies with colors of $R - i = 0.7 \pm 0.3$ as possible cluster members, because G1 and G2 have $R - i$ colors of 0.6 and 0.8, respectively. The $R - i$ color of 0.7 is consistent with the red-sequence color of a galaxy cluster at $z \sim 0.55$ (e.g., Goto et al. 2003). The selected galaxies are plotted as dark filled circles in the right panel of Figure 1. As expected, clustering of galaxies near G1 and G2 is much more pronounced after the color cut, suggesting the existence of a cluster of galaxies at $z \sim 0.55$.

3. DISCUSSION AND CONCLUSION

An interesting thing about this lens system is that the quasar images and the light center of the lensing cluster appear not to be collinear (see Figure 1). Brightest cluster galaxies are sometimes significantly offset from the center of a cluster mass (e.g., Lin & Mohr 2004), so the lack of collinearity does not necessarily argue against the lensing hypothesis. Nevertheless, it is of great interest to understand the impact of this offset for lens models. To explore this, we use standard mass modeling techniques as implemented in the public *lensmodel* software (Keeton 2001). Since the small number of observational constraints limits detailed investigations of the mass distribution, we adopt the simplest model used for modeling studies, a singular isothermal ellipsoid (SIE). We fit the quasar positions and fluxes assuming a position error of $0''.5$ and a flux error of 20%; we adopt errors larger than the actual measurement errors in order to account for perturbations from massive galaxies in the cluster. In addition we include a mild prior on the ellipticity, $e = 0.3 \pm 0.2$, to exclude models with a highly elongated cluster. With this model, we derive the allowed range for the center position of the lensing cluster potential, as shown in Figure 3. The offset of at least $\sim 30 \text{ kpc}$

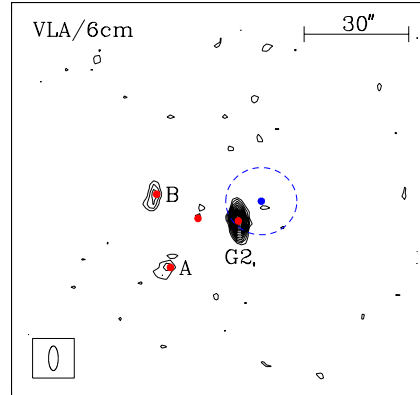


FIG. 4.— The 6 cm VLA radio map of SDSS J1029+2623 field. North is up and East is left. The observation was made during the transition between the B and CnB arrays, leading to the strongly elongated beam (shown in the lower left inset). The red small dots represent the optical position of components A, B, G1, and G2. The small blue dot Northwest of G2 marks the ROSAT X-ray source position while the surrounding blue dashed circle indicates the uncertainties in the position.

between the preferred model positions and galaxies G1 and G2 suggests either that the actual mass distribution of the lensing cluster is more complex than this simple model or that there is a genuine offset that might be confirmed in X-ray observations.

While the similarity of the optical spectra and the existence of the lensing galaxy cluster make the lensing interpretation solid, we can further test the lensing hypothesis using archival data at other wavelengths. In the FIRST radio survey (Becker et al. 1995), there are two radio sources in the field: Galaxy G2, with a peak flux of 4.20 mJy/beam, is the strongest source, component B, with a peak flux of 1.01 mJy/beam, is detected just at the flux limit, and component A is not detected. Although the difference could be explained by quasar variability combined with the time delay between the lensed images, it might argue a binary interpretation for the quasars. In order to clarify the interpretation of the FIRST radio data, we obtained a 1 hour 6 cm Very Large Array (VLA) radio map of the system on 23 September 2006. Figure 4 shows the primary beam corrected VLA 6 cm map; both quasar components have more than 5σ detections ($0.237 \pm 0.045 \text{ mJy/beam}$ for A and $0.325 \pm 0.045 \text{ mJy/beam}$ for B). There are some offsets (but within 5σ , see Table 1) between the SDSS positions and the VLA positions of the quasar components. However both components are extended in the VLA data and better quality data will be necessary to clarify the offsets. The radio loudnesses of the images, defined relative to the SDSS i -band fluxes, are 1.8 and 2.5 for images A and B, respectively. The radio flux ratio (A/B) of 0.73 is mildly inconsistent with the optical flux ratio of 1.2, however, allowing for variability both between the epochs of the two observations and the multi-year time delay of the two images, finding two quasars with such similar radio loudnesses further supports the lensing hypothesis given the enormous range of radio loudnesses observed for quasars (Ivezić et al. 2002).

The system was also detected as 1RXS

J102912.0+262338 by the ROSAT All-Sky Survey (Voges et al. 1999) with a count rate of 0.040 ± 0.016 counts s^{-1} . This corresponds to an 0.1-2.4 keV flux of approximately $(4 \pm 1) \times 10^{-13}$ ergs $cm^{-2} s^{-1}$, and it is flagged as an extended source, albeit at low significance. The X-ray position could be consistent with the position of G2 given the $10''.0$ uncertainties in the X-ray data (Figure 4). Assuming the X-ray signals arise from the lensing cluster ($z \sim 0.55$), the X-ray luminosity is approximately $3 \times 10^{44} h^{-2}$ ergs s^{-1} (for a cosmological model with $\Omega_M = 0.3$ and $\Omega_\Lambda = 0.7$) and corresponds to a velocity dispersion of approximately $\sigma \simeq 1000$ km s^{-1} that is slightly larger than the velocity scale of $\sigma \simeq 900$ km s^{-1} needed to produce the $22''.5$ image separation. Thus the X-ray luminosity is a little too high, suggesting that the AGN in galaxy G2 is an X-ray source as well as a radio source, even though it shows no signs of AGN activity in its broad band optical colors.

In summary, the best interpretation of the two quasar components in the SDSS J1029+2623 system is that a quasar at $z_s = 2.197$ is doubly imaged by a cluster of galaxies at $z_l \sim 0.55$. The evidence for strong lensing comes from the remarkable similarity of the spectral shapes and the similar radio loudnesses of the two quasars, and the existence of the lensing cluster with the presence of an extended X-ray source which is capable of producing the observed image separation. However, simple mass models require a center of the cluster potential offset from the positions of the bright galaxies or the ROSAT X-ray emission. Such an offset with respect to the bright galaxies was also found for the SDSS1004+4112 system (Oguri et al. 2004), and the X-ray position may be dominated by the AGN in galaxy G2. Thus, further follow-up observations, such as deep and high-resolution X-ray imaging and optical spectroscopy of member galaxies are needed to identify the cluster potential center.

This work was supported in part by Department of

Energy contract DE-AC02-76SF00515. A portion of this work was also performed under the auspices of the U.S. Department of Energy, National Nuclear Security Administration by the University of California, Lawrence Livermore National Laboratory under contract No. W-7405-Eng-48. The National Radio Astronomy Observatory is a facility of the National Science Foundation operated under cooperative agreement by Associated Universities, Inc. This work made use of the Very Large Array at the NRAO, and we thank NRAO for a rapid response time award.

Funding for the SDSS and SDSS-II has been provided by the Alfred P. Sloan Foundation, the Participating Institutions, the National Science Foundation, the U.S. Department of Energy, the National Aeronautics and Space Administration, the Japanese Monbukagakusho, the Max Planck Society, and the Higher Education Funding Council for England. The SDSS Web Site is <http://www.sdss.org/>.

The SDSS is managed by the Astrophysical Research Consortium for the Participating Institutions. The Participating Institutions are the American Museum of Natural History, Astrophysical Institute Potsdam, University of Basel, Cambridge University, Case Western Reserve University, University of Chicago, Drexel University, Fermilab, the Institute for Advanced Study, the Japan Participation Group, Johns Hopkins University, the Joint Institute for Nuclear Astrophysics, the Kavli Institute for Particle Astrophysics and Cosmology, the Korean Scientist Group, the Chinese Academy of Sciences (LAMOST), Los Alamos National Laboratory, the Max-Planck-Institute for Astronomy (MPIA), the Max-Planck-Institute for Astrophysics (MPA), New Mexico State University, Ohio State University, University of Pittsburgh, University of Portsmouth, Princeton University, the United States Naval Observatory, and the University of Washington.

REFERENCES

- Abazajian, K., et al. 2003, *AJ*, 126, 2081
 Abazajian, K., et al. 2004, *AJ*, 128, 502
 Abazajian, K., et al. 2005, *AJ*, 129, 1755
 Adelman-McCarthy, J. K., et al. 2006, *ApJS*, 162, 38
 Bartelmann, M., Meneghetti, M., Perrotta, F., Baccigalupi, C., & Moscardini, L. 2003, *A&A*, 409, 449
 Becker, R. H., White, R. L., & Helfand, D. J. 1995, *ApJ*, 450, 559
 Bertin, E. & Arnouts, S. 1996, *A&AS*, 117, 393
 Blanton, M. R., Lin, H., Lupton, R. H., Maley, F. M., Young, N., Zehavi, I., & Loveday, J. 2003, *AJ*, 125, 2276
 Csabai, I., et al. 2003, *AJ*, 125, 580
 Fohlmeister, J., et al. 2006, *ApJ*, submitted (astro-ph/0607513)
 Fukugita, M., Ichikawa, T., Gunn, J. E., Doi, M., Shimasaku, K., & Schneider, D. P. 1996, *AJ*, 111, 1748
 Goto, T., et al. 2003, *AJ*, 123, 1807
 Gunn, J. E., et al. 1998, *AJ*, 116, 3040
 Gunn, J. E., et al. 2005, *AJ*, 131, 2332
 Hennawi, J. F., Dalal, N., & Bode, P. 2006, *ApJ*, in press (astro-ph/0506175)
 Hogg, D. W., Finkbeiner, D. P., Schlegel, D. J., & Gunn, J. E. 2001, *AJ*, 122, 2129
 Inada, N., et al. 2003, *Nature*, 426, 810
 Ivezić, Ž., et al. 2002, *AJ*, 124, 2364
 Ivezić, Ž., et al. 2004, *AN*, 325, 583
 Kashikawa, N., et al. 2002, *PASJ*, 54, 819
 Kawano, Y., & Oguri, M. 2006, *PASJ*, 58, 271
 Keeton, C. R. 2001, preprint (astro-ph/0102340)
 Kochanek, C. S. 2002, *ApJ*, 578, 25
 Kochanek, C. S. 2006, in: Kochanek, C. S., Schneider, P., Wambsganss, J., Part 2 of Gravitational Lensing: Strong, Weak & Micro, Proceedings of the 33rd Saas-Fee Advanced Course, G. Meylan, P. Jetzer & P. North, (eds.), Springer-Verlag: Berlin, 91
 Lin, Y.-T., & Mohr, J. J. 2004, *ApJ*, 617, 879
 Lupton, R. H., Gunn, J. E., & Szalay, A. S. 1999, *AJ*, 118, 1406
 Lupton, R., Gunn, J. E., Ivezić, Z., Knapp, G. R., Kent, S., & Yasuda, N. 2001, in ASP Conf. Ser. 238, *Astronomical Data Analysis Software and Systems X*, ed. F. R. Harnden, Jr., F. A. Primini, and H. E. Payne (San Francisco: Astr. Soc. Pac.), p. 269
 Oguri, M., et al. 2004, *ApJ*, 605, 78
 Oguri, M., & Keeton, C. R. 2004, *ApJ*, 610, 663
 Oguri, M., et al. 2006, *AJ*, 132, 999
 Pier, J. R., Munn, J. A., Hindsley, R. B., Hennessy, G. S., Kent, S. M., Lupton, R. H., & Ivezić, Ž. 2003, *AJ*, 125, 1559
 Richards, G. T., et al. 2002, *AJ*, 123, 2945
 Sharon, K., et al. 2006, *ApJ*, 629, L73
 Smith, J. A., et al. 2002, *AJ*, 123, 2121
 Stoughton, C., et al. 2002, *AJ*, 123, 485
 Tucker, D. L., et al. 2006, *AN*, in press (astro-ph/0608575)
 Voges, W., et al. 1999, *A&A*, 349, 389
 Wambsganss, J. 2003, *Nature*, 426, 781
 Williams, L. L. R., & Saha, P. 2004, *AJ*, 128, 2631
 York, D. G., et al. 2000, *AJ*, 120, 1579

TABLE 1
 PROPERTIES OF SDSS J1029+2623

Component	R.A.(SDSS)	Decl.(SDSS)	R.A.(VLA)	Decl.(VLA)	i	$u - g$	$g - r$	$r - i$	$i - z$	Redshift ^a
A	10:29:13.94	+26:23:17.9	10:29:14.05 ^b	+26:23:17.4 ^b	18.59±0.01	0.72±0.04	0.18±0.01	0.19±0.01	0.32±0.03	2.1966±0.0003
B	10:29:14.24	+26:23:40.1	10:29:14.31 ^b	+26:23:39.3 ^b	18.61±0.01	0.67±0.04	0.14±0.01	0.20±0.01	-0.10±0.04	2.1969±0.0003
G1	10:29:13.35	+26:23:32.8	19.01±0.04	0.71±0.90	1.93±0.17	1.05±0.06	0.75±0.09	0.56±0.03
G2	10:29:12.48	+26:23:32.0	10:29:12.49	+26:23:31.9	18.77±0.03	1.63±1.72	1.87±0.15	1.06±0.05	0.48±0.08	0.53±0.06

NOTE. — Data are from the SDSS except for the celestial coordinates in the VLA data and the spectroscopic redshifts. Magnitudes refer model magnitudes without Galactic extinction corrections, measured on 13 December 2004. All celestial coordinates are given in J2000.

^aSpectroscopic redshifts (derived from Mg II emission lines in the FOCAS spectra) for A and B, and photometric redshifts for G1 and G2 (Csabai et al. 2003).

^bVLA position errors for A and B are both about 0'5 per coordinate.